Spatial and temporal changes of SO_2 regimes over China in recent decade and the driving mechanism

Ting Wang[1], Pucai Wang[1, 3], Nicolas Theys[2], Dan Tong[4], François Hendrick[2], Qiang Zhang[4], Michel Van Roozendael[2]

1 CAS Key Laboratory of Middle Atmosphere and Global Environment Observation, Institute of Atmospheric Physics, Chinese Academy of Sciences, Beijing, China

2 Belgian Institute for Space Aeronomy (IASB-BIRA), Brussels, Belgium

3 University of Chinese Academy of Sciences, Beijing 100049, China

4 Ministry of Education Key Laboratory for Earth System Modeling, Department of Earth System Science, Tsinghua University, Beijing, China

Revised, *Atmos Chem Phys*

Correspondence to:

Ting Wang, Institute of Atmospheric Physics, Chinese Academy of Sciences, Beijing 100029, E-mail: wangting@mail.iap.ac.cn

Abstract: The spatial and temporal changes of SO_2 regimes over China during 2005 to 2016 and their associated driving mechanism are investigated based on a state-of-the-art retrieval dataset. Climatological SO_2 exhibits pronounced seasonal and regional variations, with higher loadings in wintertime and two prominent maxima centered in the North China Plain and the Cheng-Yu District. In the last decade, overall SO_2 decreasing trends have been reported nationwide, with spatially varying downward rates according to a general rule—the higher the SO_2 loading, the more significant the decrease. However, such decline is in fact not monotonic, but instead four distinct temporal regimes can be identified by empirical orthogonal function analysis. After an initial rise at the beginning, SO_2 in China undergoes two sharp drops in the periods 2007-2008 and 2014-2016, amid which 5-year moderate rebounding is sustained. Despite spatial coherent behaviors, different mechanisms are tied to North China and South China. In North China, the same four regimes are detected in the time series of emission that is expected to drive the regime of atmospheric SO_2, with a percentage of explained variance amounting to 81%. Out of total emission, those from industrial sector dominate SO_2 variation throughout the whole period, while the role of household emission remains uncertain. In contrast to North China, SO_2 emissions in South China exhibit a continuous descending tendency, due to the coordinated cuts of industrial and household emissions. As a result, the role of emissions only makes up about 45% of the SO_2 variation, primarily owing to the decoupled pathways of emission and atmospheric content during 2009 to 2013 when the emissions continue to decline but atmospheric

content witnesses a rebound. Unfavorable meteorological conditions, including deficient precipitation, weaker wind speed and increased static stability, outweigh the effect of decreasing emissions and thus give rise to the rebound of SO_2 during 2009 to 2013.

Key words: SO_2, China, spatiotemporal regimes, mechanism, emission inventory, meteorological condition

1 Introduction

In recent decade, air pollution has persistently plagued China, especially in leading economic and densely populated areas (Chan and Yao 2008; Ma et al., 2012; Chai et al., 2014). In China, environmental protection agencies identify six major pollutants of concern, including sulfur dioxide (SO_2), nitrogen dioxide (NO_2), ozone (O_3), carbon monoxide (CO), fine particulate matter (PM2.5) and coarse particulate matter (PM10). Then, values of the six pollutants are transformed into a single number called Air Quality Index (AQI) for effective communication of air quality status and corresponding health impact (MEPC, 2012).

SO_2 is one of the six major pollutants in China (Ren et al., 2017). It is harmful to human health, affecting lung function, worsening asthma attacks and aggravating existing heart disease (WHO, 2018). It also leads to the acidification of the atmosphere, and the formed sulfate aerosol is one of the most important components of fine particles in cities (Meng et al., 2009). Overall, SO_2 is a key influencing factor for atmospheric pollution, and it poses great threats to life, property and environment (Wang et al., 2014).

Compared to airborne and ground-based remote sensing, satellite platforms permit near-global coverage on a continuing and repetitive basis, enabling quick and large-scale estimation of pollution patterns (Yu et al., 2010). Since the world's first weather satellite TIROS-I launched in 1960, satellites have become a crucial part of Earth's observations and practical applications (Yu et al., 2010). Till now, SO_2 has been measured globally by several operational satellite instruments, such as OMPS (Zhang

et al., 2017), GOME-2 (Munro et al., 2006; Rix et al., 2012) and OMI (Lee et al., 2011; Li et al., 2013; Theys et al., 2015).

With the aid of satellite data, in the past decade, various attempts have been made to explore the variation of SO_2 loadings in China. Lu et al. (2010) report that total SO_2 emissions in China have increased by 53% from 2000 to 2006, followed by a growth rate slowdown and the start of a decrease. Li et al. (2010), Yan et al. (2014), and Zhang et al. (2012) all highlight the prominent reduction of SO_2 during 2007 and 2008, as a consequence of the widespread deployment of flue-gas desulfurization and the strict control strategy implemented for preparation of the 2008 Olympic Games. Throughout the past decade, 90% of the locations in China have shown a decline in SO_2 emissions, as highlighted by Koukouli et al. (2016). Such widespread declines are ascribed to effective air quality regulations enforced in China (van der A et al., 2017). Furthermore, Krotkov et al. (2016) and Li et al. (2017) both compared the sulfurous pollution in China and India, and pointed out their opposite trajectories. Since 2007, emissions in China have declined while those in India have increased substantially. Nowadays, India is overtaking China as the world's largest emitter of anthropogenic SO_2. In addition, several studies conducted analyses on SO_2 in sub-regions of China, for example Jin et al. (2016), Lin et al. (2012), Wang et al. (2015) and Su et al. (2011). All these studies contributed to a better understanding of SO_2 changes in China. However, there are still key issues to be addressed. First, with the pace of considerable progress made on SO_2 retrieval, updated data products are now available to accurately derive recent SO_2

variations in China. Second, although the general decreasing tendency has been revealed, the specific spatial and temporal regimes remain unclear. Does the SO_2 decrease monotonically, or is there a complicated oscillation? How similar/different are SO_2 variations in different parts of the country? Third, there is more to be learned about the driving mechanisms that govern SO_2 variations. Previous studies have mainly focused on the impact from amounts of emission. However, the SO_2 content is not only dependent on emissions but also on atmospheric conditions. Therefore, how large is the influence of atmospheric variability on the variation of SO_2?

The overall goal of this study is to quantify the spatial and temporal changes of SO_2 regimes over China in the last decade and to disclose the driving mechanism, based on a new-generation of SO_2 retrieval dataset (Theys et al., 2015). Figure S1 labels the provinces of China. The manuscript is organized as follows. Section 2 describes the new SO_2 product, and emission inventories and atmospheric data are introduced. In Section 3, we evaluate the general patterns of SO_2 including mean distribution, long-term trends and seasonality. Subsequently, Section 4 identifies the specific regimes of SO_2 variability and the associated driving mechanisms. Finally, concluding remarks and future directions are presented in Section 5 and Section 6, respectively.

2 Data

2.1 SO_2 VCD retrievals

The Ozone Monitoring Instrument (OMI) is one of four sensors onboard the Aura

115 satellite launched in July 2004 (Levelt, J. et al., 2006). In recent years, Belgian Institute
116 for Space Aeronomy (BIRA) and cooperators have developed an advanced Differential
117 Optical Absorption Spectroscopy (DOAS) scheme to improve the retrieval accuracy of
118 SO_2 in troposphere. A SO_2 vertical column product is generated based on the algorithm
119 applied to OMI-measured radiance spectra (Theys et al. 2015). The retrieval scheme is
120 a based on a DOAS approach, including three steps: (1) a spectral fit in the 312-326 nm
121 range (other fitting windows are used for volcanic scenarios but are not relevant for this
122 study), (2) a background correction for possible bias on retrieved SO_2 slant columns,
123 (3) a conversion into SO_2 vertical columns through radiative transfer air mass factors
124 calculation, accounting for the SO_2 profile shape (from the IMAGES chemistry
125 transport model), geometry, surface reflectance and clouds.
126 Compared to the BRD OMI NASA SO_2 product, the BIRA retrievals proved to be
127 better both in terms of noise level and accuracy. The BIRA product is also fully
128 characterized (errors, averaging kernels, etc.). The improved OMI PCA SO_2 product of
129 NASA show similar performance and long-term trends as the BIRA product. The BIRA
130 SO_2 product has been validated in China with long-term MAX-DOAS data (Theys et
131 al., 2015; Wang et al., 2017).
132 The dataset is made available on a 0.25° and 0.25° regular latitude-longitude grid
133 over the rectangular domain 70-140°E, 10-60°N, and covers the period of 2005 to 2016
134 at monthly interval. In addition, a cloud screening is applied to remove measurements
135 with a cloud fraction of more than 30%. Other details can be found in Theys et al. (2015).

Given that missing values are often presented in satellite-retrieved product due to the limitations of retrieval algorithms under adverse environments, it is necessary to evaluate the availability of monthly SO_2 data relative to the entire period. As mapped in Figure S2, there appears to be a substantial fraction of data gaps in western and northeastern China, especially in the winter half year. This can be attributed to snow cover surfaces and high solar zenith angles, which invalidate the measurability. As a result, it may be problematic when sampling western and northeastern China. In contrast, the completeness across eastern parts of China is generally more than 80% regardless of the season, sufficient for inferring the spatial and temporal structures. In what follows, the analysis is mainly confined to the eastern China to avoid issues related to missing data.

2.2 Emission Inventory

The SO_2 emissions at national and provincial level are collected from the China Statistical Yearbook on Environment, which is compiled jointly by the National Bureau of Statistics and Ministry of Environmental Protection. It is an annual statistics publication, with industrial and household emissions listed separately. Currently, this publicly available dataset spans the period from 2003 to 2015, covering 31 provinces in China other than Taiwan, Hong Kong and Macau. Industrial emissions refer to the volume of SO_2 emission from fuel burning and production processes in the premises of enterprises for a given period, while household emissions are calculated on the basis of consumption of coal by households and the sulphur content of coal. Notice that power

157 generation is incorporated into industrial sources and emissions from transportation
158 sources are not reported. This emission inventory released in the official yearbook
159 (OYB for short) has been cited or used in several works, i.e. Li et al. (2017), Yan et al.
160 (2017), Hou et al. (2018), and etc.

161 Since a credible emission inventory is the key foundation of this study, the Multi-
162 resolution Emission Inventory for China (MEIC) developed by Tsinghua University (Li
163 et al., 2017; Zheng et al., 2018) has been adopted to verify the OYB inventory as well
164 as to corroborate our findings. The MEIC is a bottom-up emission inventory model
165 including more than 700 anthropogenic sources and then aggregated into five sectors:
166 power, industry, residential, transportation and agriculture. Unlike the OYB estimate,
167 emissions from power plants in MEIC are considered to be a single sector and presented
168 separately. Here, we use province-level emissions from 2003 to 2015, together with the
169 monthly gridded emissions at 0.25º×0.25º horizon resolution for the years 2008, 2010,
170 2012, 2014 and 2016. To be in line with the OYB inventory, transportation and
171 agriculture sectors are excluded when calculate summed emission, and the power sector
172 is folded into industrial sector.

173 Figure 1 compares the OYB and MEIC emission inventories in terms of both national
174 and regional scales. In addition, the other two candidates on national annual totals
175 including REASv2 (Kurokawa et al., 2013) and Zhao (Xia et al., 2016) are overlaid.
176 Figure 1a shows that considerable differences exist with regards to the magnitude
177 among the four datasets and in particular OYB emissions are generally lower than those

deduced from other inventories. However, their temporal variations are characterized in a very similar manner. As further illustrated in the scatter plot of OYB against the other three (Figure 1b), highly linear clustered markers with correlations above 0.92 confirm such temporal consistency. On even smaller regional scale, as shown in Figure 1c, high degrees of correspondence between OYB and MEIC overwhelm the whole eastern China, with most correlations exceeding the 0.05 significant level. In comparison, the western China features relatively less agreement, but it is not a major concern in this study.

In short, all the datasets capture coherent temporal behaviors, despite the spread in their magnitudes. We emphasize that this study is centered on the fluctuation patterns rather than the magnitude itself. Therefore, the above evidences justify the use of the OYB dataset in the following text. Meanwhile, in order to test whether results were robust to using a different data set, all analyses have been repeated using the MEIC inventory.

2.3 Meteorological Fields

The large-scale meteorological conditions are taken from Japanese 55-year Reanalysis (JRA-55) data, prepared by the Japan Meteorological Agency (Kobayashi et al., 2015; Harada et al., 2016). The variables analyzed include total column precipitable water, horizontal wind and temperature at pressure levels.

3 General patterns of SO_2 over China

3.1 Mean distribution

Based on 12 years of SO_2 column data over China, Figure 2a shows the spatial pattern of long-term mean. Overall, SO_2 distribution is of great inhomogeneity in China, with two maximum centers: one is the North China Plain (NCP for short), and the other is Cheng-Yu (CY) district in Southwest China. In particular, SO_2 amount in NCP exceeds 1.2 DU. There are two essential causes responsible for high SO_2 loading in the two areas. On the one hand, combined effect of rapid economic and industrial development as well as population growth leads to a high degree of anthropogenic SO_2 emission. Figure 2c and Figure 2d show the emission strengths, defined as emitted SO_2 per unit area, in each province based on OYB and MEIC respectively. Note that in the rest of this paper, the terms "emission" or "emission amount" always refers to "per unit area emission". It is obvious that the two regions release above 8.0 tons/km^2 SO_2 per year, which is three times greater than the average level of China. Although OYB exhibits smaller magnitude of emissions than MEIC, the spatial patterns in terms of relative difference across space are generally consistent. On the other hand, as shown in Figure 2b, either of the two regions is surrounded or partly surrounded by mountains, which makes it difficult for the pollutants to dissipate.

In contrast, over the sparsely populated western part of China, low SO_2 concentrations of less than 0.2 DU are observed, except over some provincial capitals. Since western part of China is less affected by human activities, anthropogenic sources

of SO_2 are much smaller than natural emissions including emissions from terrestrial ecosystems and oxidation of H_2S to SO_2 (Wang et al., 1999). Between latitude 30-40°N, for example, the SO_2 amount over the eastern regions (110-120°E) are 6-12 times greater than western regions (80-110°E). In addition, note that the low-level SO_2 columns in western China are subject to large uncertainties and the background correction is an important source of error. However, the western China with weak SO_2 signals/background SO_2 is not the subject of the present work, since we mainly focus on the highly polluted eastern China.

Besides the NCP and CY regions with highest SO2 loadings, this study is also interested in Yangtze River Delta (YRD) and Pearl River Delta (PRD), the other two economic mega-urban zones in China. These four identified hotspots NCP, CY, YRD and PRD are outlined in Figure 2a and will be specially examined in the following discussion.

3.2 Seasonal Cycle

The annual total is decomposed into seasonal cycle, as shown in Figure 3. In eastern China, about 35% of the annual totals is from winter, while SO_2 in summer only accounts for 15%; the remaining 50 percent is almost equally divided in spring and autumn. Seasonal variations measured in the fractional contribution are similar within eastern China.

To unveil the underlying mechanism, Figure 4 illustrates the annual cycle of SO_2 VCDs in relation to sulphur emission, precipitable water and temperature at the four

hotspots. Intensive heating during winter in North China raises sulphur release. However, emissions alone are not sufficient to explain the pronounced seasonality of SO_2. The remaining variation is associated with the seasonal change of the meteorological conditions. Temperature and humidity are cold and dry in winter due to the influence of winter monsoon, which jointly weaken the rate of oxidation and wet deposition. Thus, one expects that SO_2 molecules will have a longer lifetime and therefore will accumulate easier. The opposite is true for summer, when chemical reaction is active and wet removal is effective. In summary, both emission and meteorological change explain the seasonality of the atmospheric SO_2 loadings.

Due to the climate transition from southern China to northern China, the annual range of SO_2 rises progressively from south to north. NCP has the greatest amplitude of up to 1 DU, while there is virtually no annual cycle in PRD. Larger amplitude for SO_2 cycles in NCP arises from the significantly reversed source-sink imbalance between summer and winter. In contrast, the climate in PRD is characterized by smoother transition over the whole year and there is no heating season, which explains the insignificant seasonal variation of SO_2 in PRD. The other two regions CY and YRD have approximately the same amplitude of 0.6 DU, because they are on the same line of latitude.

3.3 Long-term trends

Figure 5 depicts the spatial pattern of linear trends in annual and seasonal SO_2 from 2005 to 2016. Overall, apparent downward trends overwhelm most parts of eastern China, while western China has experienced little change. In particular, the most

261 significant reduction occurred in the highly SO_2-polluted regions, with the decreasing
262 rates amounting to 0.1 DU/a. This result suggests that the governments and
263 communities in these economically developed regions have done its best to effectively
264 control environmental pollution, including energy saving, emission cut and adjustment
265 of energy consumption structure, shutdown of the most polluting factories, upgradation
266 of coal quality, etc. Besides, enforcement of environmental protection laws is becoming
267 more and more rigorous (van der A et al., 2017). Therefore, under collaborative efforts,
268 the SO_2 levels in these highly developed regions with high background concentration
269 have been decreasing markedly in the recent decade. Moreover, the pattern correlation
270 between mean (Figure 2a) and trends (Figure 5 top) of SO_2 reaches to –0.77, implying
271 that the downward rate over China can be summarized into a general rule—the higher
272 the SO_2 loading, the more significant the decrease.
273 Figure 5a-d portrays the long-term trends of SO_2 on seasonal basis. On the one hand,
274 every season has witnessed SO_2 reduction, with the strongest decrease occurring in
275 winter and autumn. Consequently, it can be concluded that the SO_2 decrease in winter
276 and autumn contribute most to the reduction of annual SO_2. On the other hand, the
277 highly SO_2-polluted regions have experienced the most pronounced decrease across all
278 seasons, which is consistent with the annual outcomes. It is noteworthy to point out that
279 a belt of large positive values extend along 40°N in winter (Figure 5a). This feature is
280 a known artefact related to the large solar zenith angles at high northern latitudes.
281 Last, we discuss the trends of the four hotspots interested. Figure 6 depicts the SO_2

columns from 2005 to 2016 as a function of year (y-axis) and calendar month (x-axis). The horizontal axis is the month of the year, the vertical axis is the year, and the color is the SO_2 VCD for that month and year. SO_2 VCDs exhibit a decreasing tendency during the last decade, regardless of the time of the year. Quantitatively, SO_2 in NCP, CY, YRD and PRD had undergone an overall downward trend with a rate of 0.062, 0.059, 0.046 and 0.055 DU per year, respectively.

4 Specific regimes of SO_2 variability and causes

4.1 Specific regimes of SO_2 variability

The above investigation presents SO_2 patterns and trends across China, but some elusive non-monotonic behaviors are not fully understood. In this section, we aim to detect the specific regimes of SO_2 variability and associated responsible mechanisms.

Spatiotemporal regimes of SO_2 over China are mapped by using empirical orthogonal function (EOF) decomposition (Hannachi, 2004), which is a useful tool to reduce the data dimensionality to two dimensions. One dimension represents the spatial structure and the other the temporal dimension. Figure 7 illustrates the leading mode (top) and the corresponding principal component (PC, bottom) obtained from EOF, since only the first mode is statistically well separated. Compared to the first EOF mode explaining 36.8% of the total variance, each of the other modes is characterized by less than 6% contribution and thus discarded. On the one side, the variation of SO_2 is dominated by a spatially uniform feature with large loadings in NCP and CY, suggesting

303 that SO_2 changes would be in the same phase but varying amplitude across the entire
304 region. On the other side, the corresponding PC exhibit overall declines during the 2005
305 to 2016. However, the result does not implicate a simple continuous decrease. In fact,
306 there appears to be a transient increase until a peak and thereafter two sharp drops occur
307 in the periods 2007-2008 and 2014-2016, amid which SO_2 concentrations are under the
308 process of slightly rebounding. In short, the SO_2 variability is characterized by four
309 distinct temporal regimes.

310 Moreover, Figure 8 demonstrates the time series for each province in eastern China,
311 with the segment over 2009-2013 highlighted by red color. It reflects extensive common
312 variation that goes through four stages—that is, a short-lived increasing period at the
313 beginning, a steep drop period during 2007 to 2008, a rebound period of 2009 to 2013
314 and another drastic drop period during 2014 to 2016. Most importantly, it confirms that
315 the SO_2 does not evolve in a monotonic way but shows a striking rebound during 2009
316 to 2013. This pattern is true throughout most of the region, with only two exceptions of
317 Guizhou and Guangdong provinces that had experienced a consecutive decrease since
318 2005.

319 **4.2 Causes**

320 In this section, we diagnose the likely mechanisms behind the observed SO_2
321 variability. Generally, emissions and meteorological conditions are two main factors
322 that essentially exert influence on atmospheric pollutant load. The impact of changes in
323 emitted SO_2, as the main driving force, is first examined. To this end, the temporal

classifications of SO_2 emission for each province based on OYB and MEIC are respectively depicted in Figure 9a and 9b, in which red upward pointing triangle implies non-monotonic decrease with a rebound in the middle whereas persistent decrease is denoted by green downward pointing triangle. In North China except Henan province, both OYB and MEIC datasets show that the emission passed its secondary peak during 2009 to 2013. In South China, however, discrepancies between OYB and MEIC emerge in some provinces, namely Jiangxi, Hunan, Guangxi and Guizhou. Even so, we are still confident enough that the majority of South China has witnessed a successive drop in emitted SO_2. In addition, an auxiliary map is presented in Figure 9c showing the slope of the linear regression of MEIC gridded emission over years 2008, 2010 and 2012. We can see that most of North China is subject to a positive rate of change while the opposite holds true over most of South China, which confirms the above findings. Eventually, it comes to conclusion that despite spatially uniformity in temporal-pattern classification of SO_2 VCD (Figure 8), temporal structure of emission demonstrates strong south-north contrast (Figure 9). Therefore, it is advantageous to treat North China and South China separately, as delineated by the dotted line in Figure 9. Regional averaged quantities are estimated as a weighted average by assigning the district area as a weight. In addition, to evade possible contaminations, we have ruled out Henan and Jiangxi provinces in OYB and Henan, Hunan, Guizhou and Guangxi provinces in MEIC.

Although we divide the eastern China into north and south blocks, the inter-regional

transport cannot be neglected. Therefore, we construct an Effective Emission Index (*EEI*) to account for impacts from both local and remote sources. Here, we directly adopt the results obtained by Zhang et al. (2015), who divided eastern China into three parts North China, Southeast China and Southwest China, and quantified the percent contributions of within-region versus inter-regional transport on sulfate concentrations. The geographical partition in their work broadly coincides with ours, with the only difference that South China is further split in two parts. Given that the ratio of Southeast China to Southwest China is 1.4, we merge the percent contributions over these two portions via simple conversions. This produces: for North China, within-region SO_2 emission contribute 68% followed by 19% from South China and 13% from other regions; for South China, within-region emissions provide 66%, while transport from North China and other regions amounts to 17% and 17% respectively. With these statistics, the *EEI* is formulated as follows:

$$\text{North China} \quad \begin{aligned} EEI_1 &= 0.68 + 0.19 + 0.13 = 1 \\ EEI_m &= 0.68 \cdot \frac{N_m}{N_1} + 0.19 \cdot \frac{S_m}{S_1} + 0.13 \end{aligned}$$

$$\text{South China} \quad \begin{aligned} EEI_1 &= 0.17 + 0.66 + 0.17 = 1 \\ EEI_m &= 0.17 \cdot \frac{N_m}{N_1} + 0.66 \cdot \frac{S_m}{S_1} + 0.17 \end{aligned}$$

where *N* and *S* denote the emission amount in North China and South China respectively, and subscripts 1 and m the 1st and m^{th} time node respectively. The fundamental assumptions to derive the formula are that *EEI* is linearly dependent on *N* and *S* and the external contributions remain fixed (without interannual variation). For comparison purpose, we also define an Emission Index (*EI*) that involves single effect from within-

365 in region emission, as written below,

366 North China $EI_1 = 1$, $EI_m = \frac{N_m}{N_1}$

367 South China $EI_1 = 1$, $EI_m = \frac{S_m}{S_1}$

368 where the notions of symbols are identical to those in *EEI* definition. In the case of
369 large scale, integrating the role of inter-regional transport does not alter the overall
370 pattern, as proved in the following analyses.

371 Figure 10 presents time series and scatter plots of SO_2 VCD and emission with its
372 variants *EI* and *EEI*, and Figure 11 is designed to show the total emission generated by
373 industries and households. These two figures are created based on OYB inventory,
374 while their counterparts obtained from MEIC inventory are shown in Figure S3 and S4
375 in the supplement material. As shown in Figure 10a, the North China features a good
376 correspondence between amount and either *EI* or *EEI*, with linear correlation of 0.9.
377 Time series of emission also indicate the existence of four distinct regimes that are
378 likely to drive the regime of SO_2 VCD directly. This is confirmed by the scatter plot
379 (Figure 10b), in which the points are tightly clustered around the regression line. Based
380 on variance analysis, emission accounts for 81% fraction of SO_2 VCD variation over
381 North China. In parallel, the same procedure relying on MEIC inventory yields nearly
382 identical results, as shown in Figure S3a and S3b. Furthermore, how large do industrial
383 and household sectors respectively contribute to the total trends? Figure 11a and Figure
384 S4a indicate that the industrial emissions play a crucial role in SO_2 VCD variation

385 throughout the whole period, while the influence induced by residential activity is
386 secondary. A more in-depth comparison between OYB and MEIC shows some
387 dissimilarity in household emission: OYB-based household emission acts to offset
388 industrial effect, while opposite function is identified for the MEIC-based one. However,
389 this does not seriously affect the major conclusion, due to the marginal impacts caused
390 by households.

391 The close linear relationship observed in North China is not found in South China,
392 since the two curves appear to become no adherent in Figure 10c and the points in the
393 scatter plot Figure 10d are widely spread around the regression line. Variance analysis
394 suggests that only 45% of SO_2 VCD variability is forced by emissions, suggesting that
395 the SO_2 variations in South China cannot be explained by emission changes alone. This
396 is mainly ascribed to the decoupled pathways of emission and SO_2 VCD during 2009
397 to 2013, as the emission continues to decline but SO_2 VCD witnesses a rebound. MEIC
398 emissions also exhibit a general decreasing tendency in spite of a transient pause
399 embedded, as shown in Figure S3c. Moreover, Figure 11b and Figure S4b suggests that
400 the cuts of industrial and household emissions collectively promote the continuous
401 decrease of total emission in South China, which are different from that in North China.
402 However, the emission decrease in the household sector is differently reported in the
403 OYB and MEIC inventories, the former one showing a sudden shift while the latter
404 displays a gradual decrease. Anyway, it is assured that household emissions in South
405 China have undergone a reduction, irrespective of the exact manner.

406 Why decreasing emissions do not cause a reduction of SO_2 VCD in South China
407 during 2009 to 2013? To answer this question, the atmospheric conditions during 2009
408 to 2013 are compared with those during the rest of the years, as depicted in Figure 12.
409 The period 2009 to 2013 is characterized by prolonged dry conditions in South China
410 with the precipitable water and precipitation being lower than usual (Figure 12a), which
411 weakens wet adsorption and scavenging. At the same time, this period is also associated
412 with relatively weaker wind speed (Figure 12b) and increased static stability (Figure
413 12c, d), reducing the ability of the atmosphere to diffuse leading to the accumulation of
414 SO_2 loads. In brief, unfavorable meteorological conditions produce the observed
415 rebound of SO_2 during 2009 to 2013, despite the continued decrease of emission.
416

417 ## 5 Conclusions

418 In this study, the spatiotemporal variability of SO_2 columns over China and the
419 associated driving mechanisms are examined over the past decade. Based on a state-of-
420 the-art SO_2 retrieval dataset recently derived from the OMI instrument, we elaborate on
421 the characteristics of specific SO_2 regimes over China and underlying causes.
422 Climatological SO_2 in China has an uneven spatial distribution in space and time.
423 East China is far more exposed to SO_2 pollution than West China, with two maxima
424 centered in NCP and CY. From analysis of the annual cycles we conclude that 35% of
425 the annual totals are from winter, while SO_2 in summer only accounts for 15% percent.
426 In addition, the annual amplitude of SO_2 rises progressively from south to north.

From 2005 through 2016, most of eastern China presents a clear decreasing tendency for SO_2, while western China has experienced little change. Spatially, the decreasing rate is generally enhanced for high SO_2 loads. When computed seasonally, SO_2 reductions in winter and autumn contribute most to the reduction of annual SO_2.

Four stages of variation are identified by EOF analysis. The first regime (2005-2006) features a transient increasing trend, the second (2007-2008) and the last (2014-2016) regimes show sharp drops, and the third regime (2009-2013) manifests itself by 5-year moderate rebounding. Although temporal regimes of SO_2 are coherent throughout the country, different driving forces are tied to North China and South China. In North China, the atmospheric SO_2 and emission varies essentially in the same way. Therefore, the atmospheric SO_2 variability is primarily associated with the emission variability, which accounts for 81% of the total variance. Further, the emission generated by industrial sector is largely responsible for the atmospheric SO_2 variability. The household emissions appears to remain uncertain, due to the dissimilarity between OYB and MEIC inventories.

SO_2 emissions in South China exhibit a continuous decreasing tendency, due to the coordinated cuts of industrial and household emissions. As a result, the role of emissions only contributes 45% of the SO_2 variation, primarily owing to the decoupled pathways of emission and atmospheric content during 2009 to 2013 when the emission continues to decline but atmospheric content witnesses a rebound. It is found that such rebound occurs in response to the joint effect of deficient precipitation, weaker wind

448 speed and increased static stability during 2009-2013.

449

450 6 Future directions

451 As enlightened by this study, the spatial and temporal changes of SO_2 regimes over
452 China in recent decade become clear. However, there is much left to be learned about
453 the responsible driving mechanisms. First, a major obstacle of cause-and-effect relation
454 surveys stems from uncertainties in the current emission inventories. In this study, many
455 facets inferred by OYB and MEIC are convergent, because we look at large spatial scale
456 and long-term general tendency that help filter out or attenuate some uncertainties.
457 However, if the aim is to focus on smaller spatial or temporal scales or on specific
458 sectors, there is still great uncertainty. To overcome these barriers, emission inventories
459 should be further improved and more observational products should be used for
460 comparison. Second, this work investigates the impact of emission, inter-regional
461 transport and meteorology using purely statistical techniques, but finer scale
462 investigations require numerical simulations using coupled chemical-transport models.
463 Third, the analysis presented in Section 4 is constrained to provincial or multi-
464 provincial levels, due to the limitation that only continuous emission data on provinces
465 are gathered at hand. In reality, however, either emission or atmospheric loadings can
466 be quite inhomogeneous within the same region. Therefore, future studies should use
467 both gridded SO_2 VCDs and gridded SO_2 emission inventories.

468

Acknowledgement: We are grateful to the editor and two anonymous reviewers for constructive comments and suggestions that greatly improve quality of this paper. This work was supported by the National Key Research and Development Program of China nos. 2017YFB0504000 and 2016YFC0200403, and the National Natural Science Foundation of China nos. 41505021 and 41575034.

7 References

Chai, F., Gao, J., Chen, Z., Wang, S., Zhang, Y., Zhang, J., Zhang, H., Yun, Y., and Ren, C.: Spatial and temporal variation of particulate matter and gaseous pollutants in 26 cities in China, Journal of Environmental Sciences, 26(1), 75-82, 2014.

Chan, C. K., and Yao, X.: Air pollution in mega cities in China, Atmospheric Environment, 42(1), 1-42, 2008.

Hannachi, A.: A primer for EOF analysis of climate data. Reading: University of Reading, 2004.

Harada, Y., and Coauthors: The JRA-55 Reanalysis: Representation of atmospheric circulation and climate variability, Journal of the Meteorological Society of Japan. Ser. II, 94(3), 269-302, 2016.

Hou, Y., Wang, L., Zhou, Y., Wang, S., Wang, F.: Analysis of the Sulfur Dioxide Column Concentration over Jing-Jin-Ji, China, based on Satellite Observations during the Past Decade, Polish Journal of Environmental Studies, 27(4), 1551-1557, 2018.

Jin, J., Ma, J., Lin, W., Zhao, H., Shaiganfar, R., Beirle, S., and Wagner, T.: MAX-DOAS measurements and satellite validation of tropospheric NO2 and SO2 vertical column densities at a rural site of North China, Atmospheric Environment, 133, 12-25, 2016.

Kobayashi, S., and Coauthors: The JRA-55 reanalysis: General specifications and basic characteristics, Journal of the Meteorological Society of Japan. Ser. II, 93(1), 5-48, 2015.

Koukouli, M. E., and Coauthors: Anthropogenic sulphur dioxide load over China as observed from different satellite sensors, Atmospheric Environment, 145, 45-59, 2016.

Krotkov, N. A., and Coauthors: Aura OMI observations of regional SO_2 and NO_2 pollution changes from 2005 to 2015, Atmospheric Chemistry and Physics, 16(7), 4605-4629, 2016.

Kurokawa, J., Ohara, T., Morikawa, T., Hanayama, S., Janssens-Maenhout, G., Fukui, T., Kawashima, K., & Akimoto, H.: Emissions of air pollutants and greenhouse gases over Asian Regions during 2000–2008: Regional Emission Inventory in Asia (REAS) version 2. Atmospheric Chemistry and Physics, 13(21), 11019–11058, 2013.

Lee, C., and Coauthors: SO_2 emissions and lifetimes: Estimates from inverse modeling using in situ and global, space‐based (SCIAMACHY and OMI) observations, Journal of Geophysical Research: Atmospheres, 116(D6), 2011.

511 Levelt, P. F., and Coauthors: The ozone monitoring instrument, IEEE Transactions on
512 Geoscience and Remote Sensing, 44(5), 1093-1101, 2006.
513 Li, C., Zhang, Q., Krotkov, N. A., Streets, D. G., He, K., Tsay, S. C., and Gleason, J. F.:
514 Recent large reduction in sulfur dioxide emissions from Chinese power plants
515 observed by the Ozone Monitoring Instrument, Geophysical Research Letters,
516 37(8), 2010.
517 Li, C., Joiner, J., Krotkov, N. A., and Bhartia, P. K.: A fast and sensitive new satellite
518 SO2 retrieval algorithm based on principal component analysis: Application to the
519 ozone monitoring instrument. Geophysical Research Letters, 40(23), 6314-6318,
520 2013.
521 Li, C., and Coauthors: India is overtaking China as the world's largest emitter of
522 anthropogenic sulfur dioxide, Scientific Reports, 7(1), 14304, 2017.
523 Li, M., and Coauthors: Anthropogenic emission inventories in China: a review,
524 National Science Review, 4(6), 834-866, 2017.
525 Lin, W., Xu, X., Ma, Z., Zhao, H., Liu, X., and Wang, Y.: Characteristics and recent
526 trends of sulfur dioxide at urban, rural, and background sites in North China:
527 Effectiveness of control measures, Journal of Environmental Sciences, 24(1), 34-
528 49, 2012.
529 Lu, Z., and Coauthors: Sulfur dioxide emissions in China and sulfur trends in East Asia
530 since 2000, Atmospheric Chemistry and Physics, 10(13), 6311-6331, 2010.
531 Ma, J., Xu, X., Zhao, C., and Yan, P.: A review of atmospheric chemistry research in

China: Photochemical smog, haze pollution, and gas-aerosol interactions. Advances in Atmospheric Sciences, 29(5), 1006-1026, 2012.

Meng, X. Y., Wang, P. C., Wang, G. C., Yu, H., and Zong, X. M.: Variation and transportation characteristics of SO2 in winter over Beijing and its surrounding areas, Climatic and Environmental Research, 14(3), 309-317, 2009. (in Chinese)

MEPC (Ministry of Environmental Protection of China): Technical regulations on ambient air quality index (on trial), 2012.

Munro, R., and Coauthors: GOME-2 on MetOp, Proc. of The 2006 EUMETSAT Meteorological Satellite Conference, Helsinki, Finland, 1216, 48, 2006.

Ren, L., Yang, W., and Bai, Z.: Characteristics of Major Air Pollutants in China, in Ambient Air Pollution and Health Impact in China, Springer, 7-26, 2017.

Rix, M., and Coauthors: Volcanic SO2, BrO and plume height estimations using GOME‐2 satellite measurements during the eruption of Eyjafjallajökull in May 2010, Journal of Geophysical Research: Atmospheres, 117(D20), 2012.

Su, S., Li, B., Cui, S., and Tao, S.: Sulfur dioxide emissions from combustion in China: from 1990 to 2007, Environmental Science and Technology, 45(19), 8403-8410, 2011.

Theys, N., and Coauthors: Sulfur dioxide vertical column DOAS retrievals from the Ozone Monitoring Instrument: Global observations and comparison to ground‐based and satellite data, Journal of Geophysical Research: Atmospheres, 120(6), 2470-2491, 2015.

van der A, R. J., Mijling, B., Ding, J., Koukouli, M. E., Liu, F., Li, Q., Mao, H., and Theys, N.: Cleaning up the air: effectiveness of air quality policy for SO2 and NOx emissions in China, Atmos. Chem. Phys., 17, 1775-1789, 2017.

Wang, S., and Coauthors: Satellite measurements oversee China's sulfur dioxide emission reductions from coal-fired power plants, Environmental Research Letters, 10(11), 114015, 2015.

Wang, T., Hendrick, F., Wang, P., Tang, G., Clémer, K., Yu, H., Fayt, C., Hermans, C., Gielen, C., Müller, J.-F., Pinardi, G., Theys, N., Brenot, H., and Van Roozendael, M.: Evaluation of tropospheric SO2 retrieved from MAX-DOAS measurements in Xianghe, China, Atmos. Chem. Phys., 14, 11149-11164, 2014.

Wang, Y., Beirle, S., Lampel, J., Koukouli, M., De Smedt, I., Theys, N., Li, A., Wu, D., Xie, P., Liu, C., Van Roozendael, M., Stavrakou, T., Müller, J.-F., and Wagner, T.: Validation of OMI, GOME-2A and GOME-2B tropospheric NO2, SO2 and HCHO products using MAX-DOAS observations from 2011 to 2014 in Wuxi, China: investigation of the effects of priori profiles and aerosols on the satellite products, Atmos. Chem. Phys., 17, 5007-5033, 2017.

WHO (World Health Organization): Ambient (outdoor) air quality and health, 2018, http://www.who.int/news-room/fact-sheets/detail/ambient-(outdoor)-air-quality-and-health.

Xia, Y., Zhao, Y., Nielsen, C.: Benefits of China's efforts in gaseous pollutant control indicated by the bottom-up emissions and satellite observations 2000–2014,

574 Atmospheric Environment, 136: 43-53, 2016.
575 Yan, H., Chen, L., Su, L., Tao, J., and Yu, C.: SO_2 columns over China: Temporal and
576 spatial variations using OMI and GOME-2 observations, IOP Conference Series:
577 Earth and Environmental Science, 17(1), 012027, 2014.
578 Yan, S., Wu, G.: SO_2 Emissions in China–Their Network and Hierarchical Structures,
579 Scientific Reports, 7, 46216, 2017.
580 Yu, H., Wang, P., Zong, X., Li, X., and Lü, D.: Change of NO_2 column density over
581 Beijing from satellite measurement during the Beijing 2008 Olympic Games,
582 Chinese Science Bulletin, 55(3), 308-313, 2010.
583 Zhang, X., van Geffen, J., Liao, H., Zhang, P., and Lou, S.: Spatiotemporal variations
584 of tropospheric SO2 over China by SCIAMACHY observations during 2004–2009,
585 Atmospheric Environment, 60, 238-246, 2012.
586 Zhang, Q., Wang, Y., Ma, Q., Yao, Y., Xie, Y., He, K.: Regional differences in Chinese
587 SO 2 emission control efficiency and policy implications, Atmospheric Chemistry
588 and Physics, 15(11), 6521-6533, 2015.
589 Zhang, Y., Li, C., Krotkov, N. A., Joiner, J., Fioletov, V., and McLinden, C.:
590 Continuation of long-term global SO2 pollution monitoring from OMI to OMPS.
591 Atmospheric Measurement Techniques, 10(4), 1495-1509, 2017.
592 Zheng, B., Tong, D., Li, M., Liu, F., Hong, C., Geng, G., Li, H., Li, X., Peng, L., Qi, J.,
593 Yan, L., Zhang, Y., Zhao, H., Zheng, Y., He, K., and Zhang, Q.: Trends in China's
594 anthropogenic emissions since 2010 as the consequence of clean air actions,

595 Atmos. Chem. Phys., doi: 10.5194/acp-2018-374, 2018.

596

597

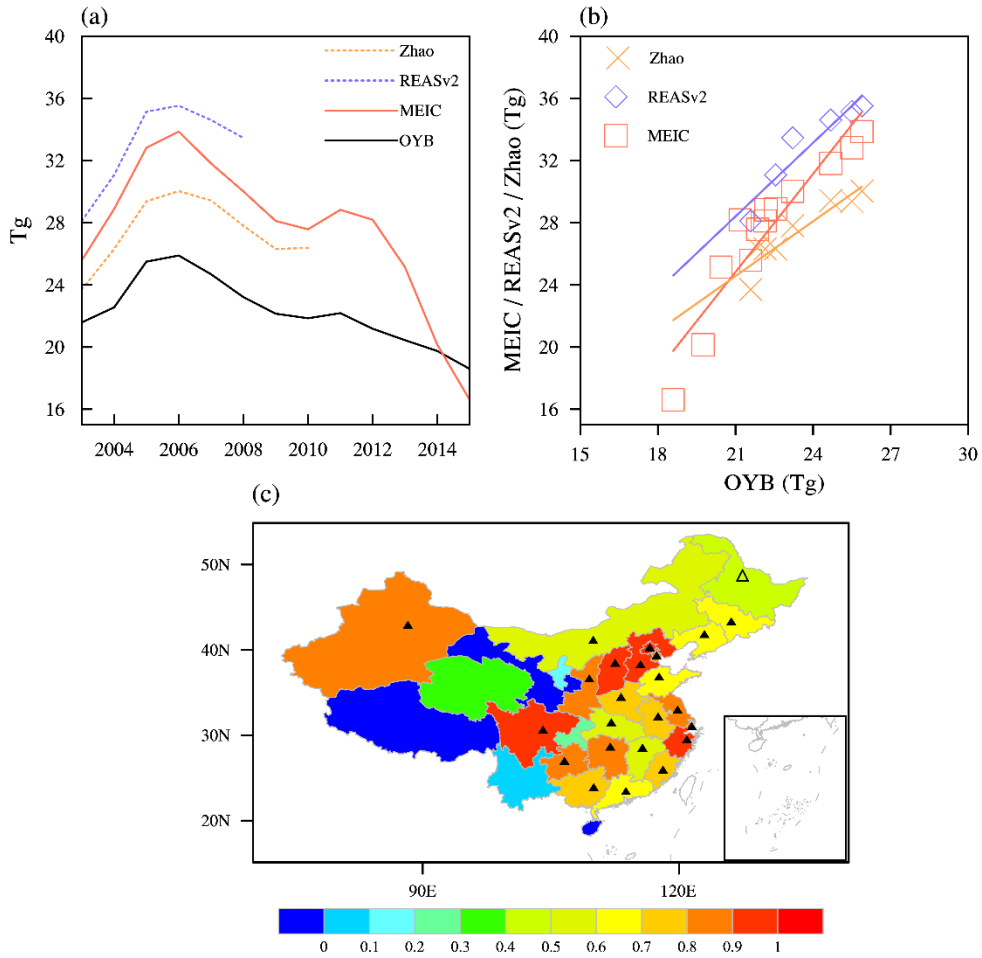

598

599 Figure 1 (a) National total SO_2 emissions estimated by OYB (solid black), MEIC (solid red), REAS

600 (dashed blue) and Zhao (dashed orange) between 2003 and 2015. (b) Scatter diagrams and regression

601 lines for OYB estimate (x-Axis) against the other three products (y-Axis). (c) The province-by-province

602 correlations between OYB and MEIC products, with the significance levels of 0.1 and 0.05 are marked

603 by open and filled triangles respectively.

604

605

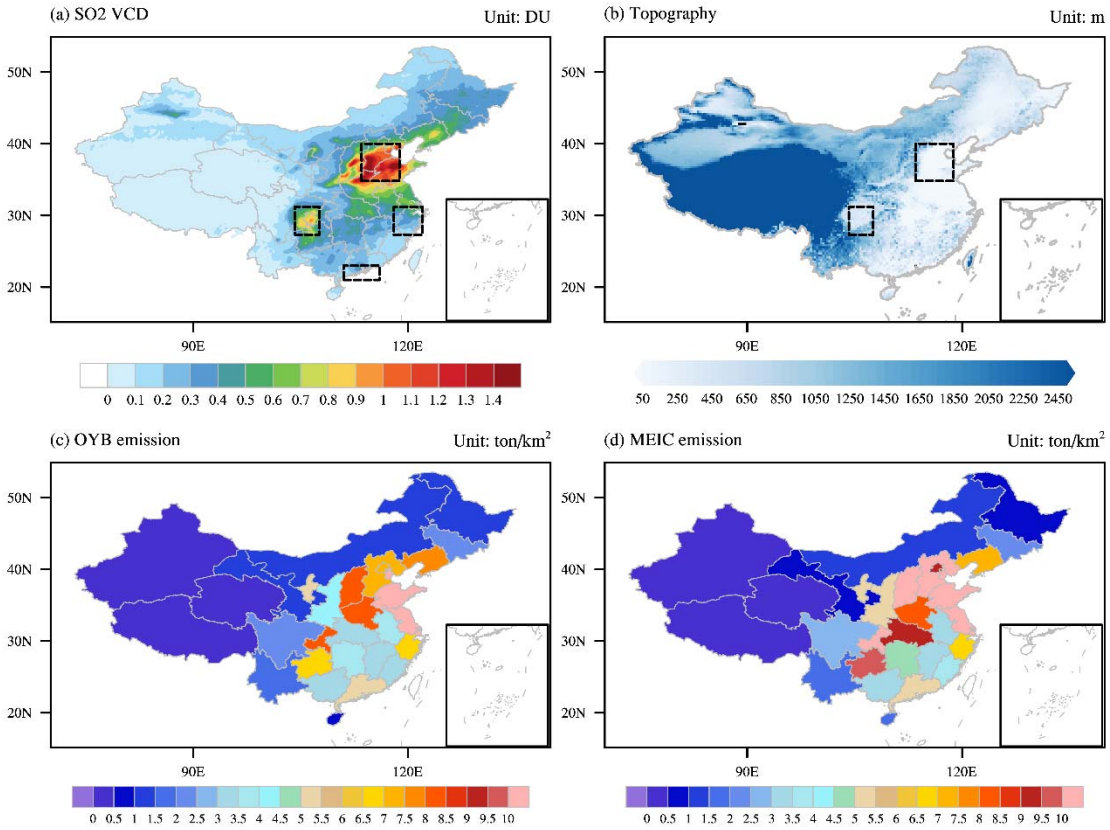

606

607 Figure 2 (a) Spatial distribution of 12-year (2005–16) averaged SO_2 columns over China. (b)

608 Topography of China in meters. (c, d) SO_2 emission (ton/km^2) among Chinese provinces based on OYB

609 and MEIC.

610

611

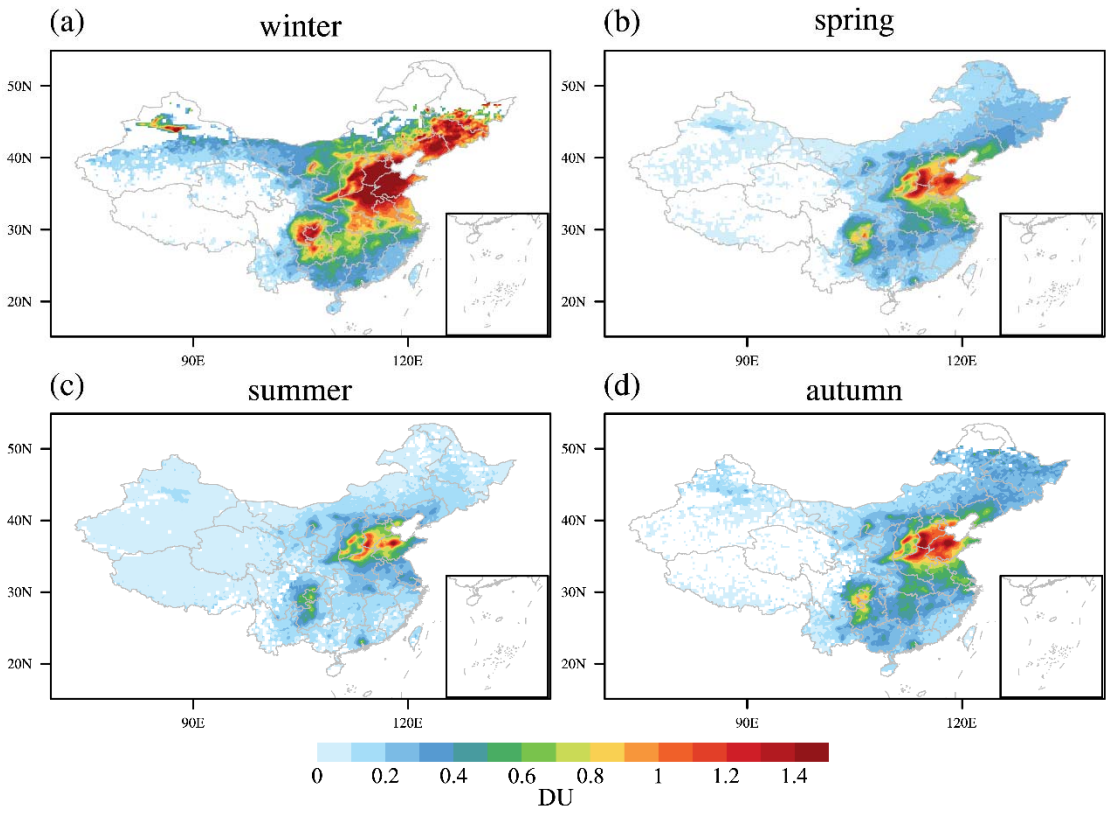

612

613 Figure 3 Seasonal SO_2 columns over China: (a) winter, (b) spring, (c) summer and (d) autumn

614

615

616

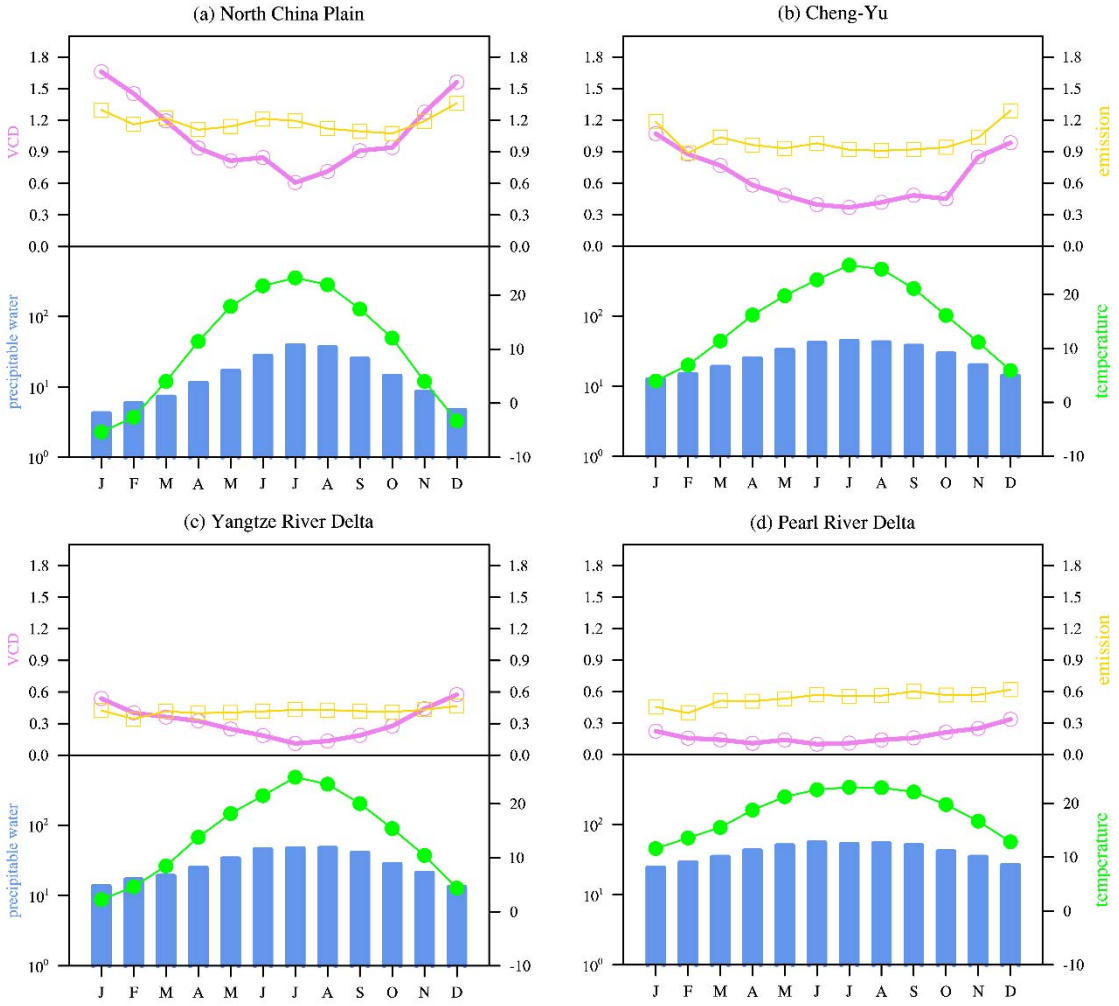

617

618 Figure 4 Annual cycle of SO_2 VCD (unit: DU, pink line), MEIC SO_2 emission (unit: ton/km^2, yellow

619 line), precipitable water (unit: kg/m^2, blue bar) and temperature at 925hPa (unit: ºC, green line) for NCP

620 (a), CY (b), YRD (c) and PRD (d).

621

622

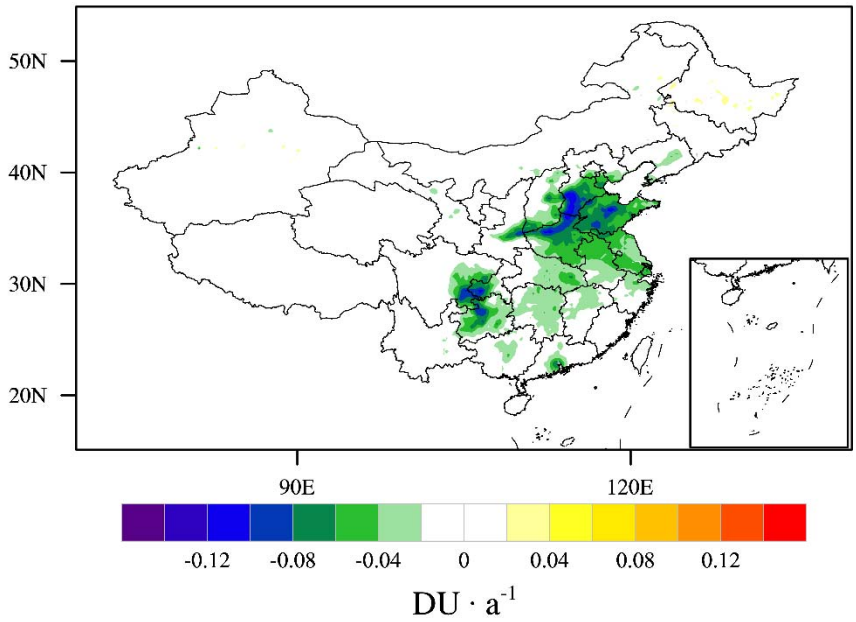

623

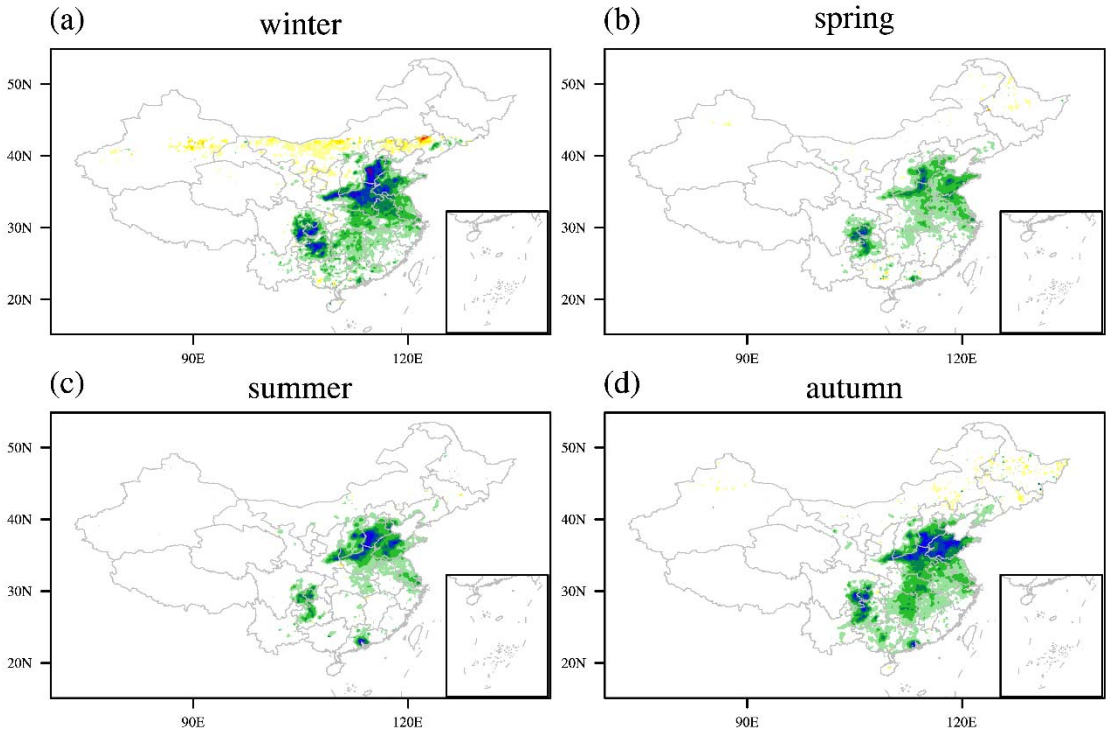

624

625 Figure 5 Spatial pattern of SO_2 linear trends (2005–16) in annual (Top) and seasonal values (a, b, c,

626 d)

627

628

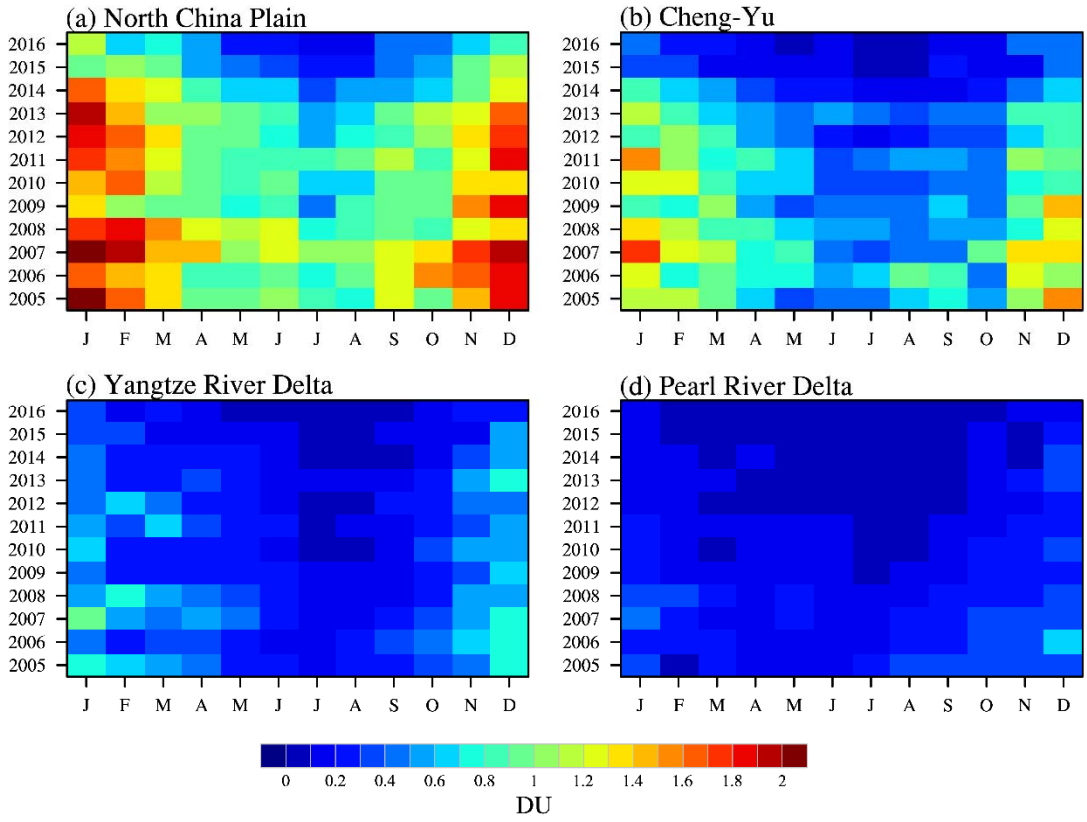

629

630 Figure 6 SO_2 amounts from 2005 to 2016 as a function of year (y-axis) and calendar month (x-axis) for

631 NCP (a), CY (b), YRD (c) and PRD (d).

632

633

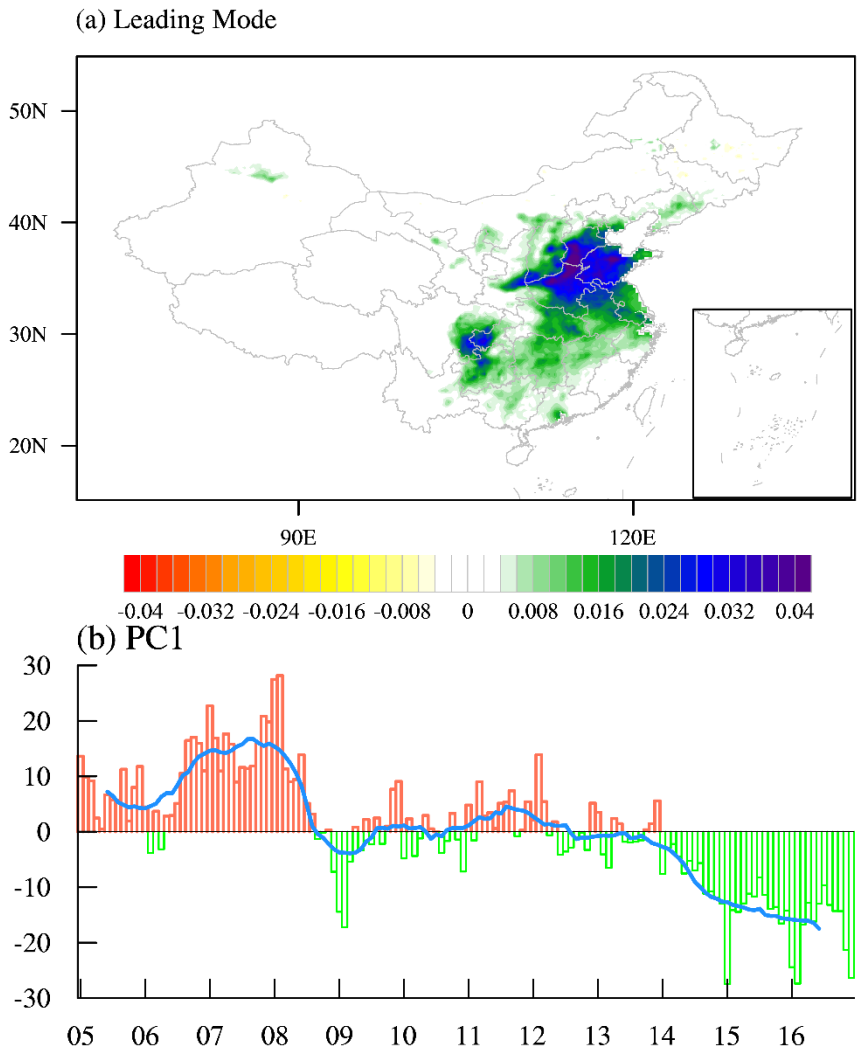

634

635 Figure 7 The first leading EOF mode (a) and the corresponding principal components (b)

636

637

638

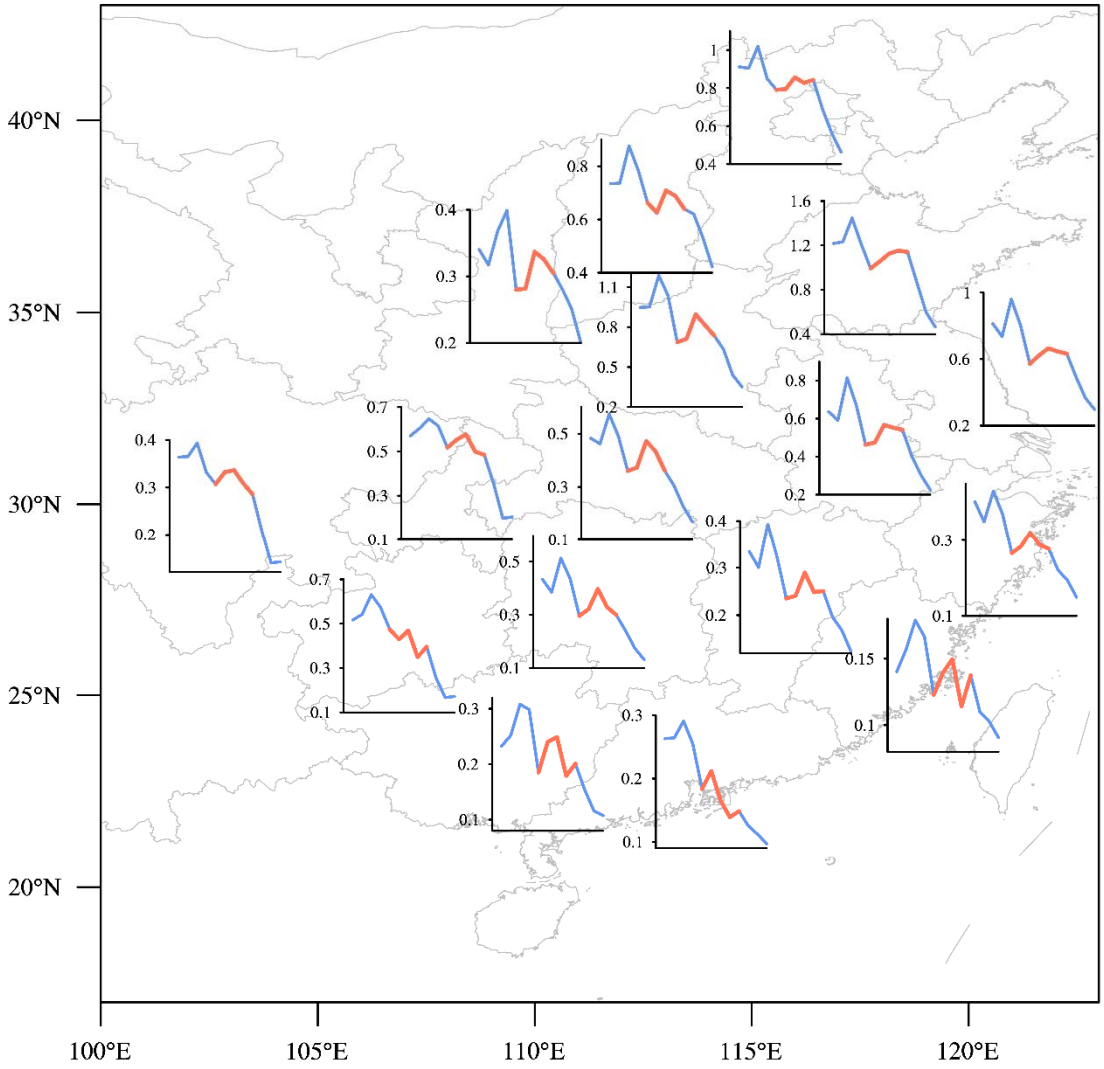

Figure 8 Temporal evolution of annual SO_2 (unit: DU) from 2005 to 2016 in each province of eastern China, with the segment over 2009-2013 highlighted by red color.

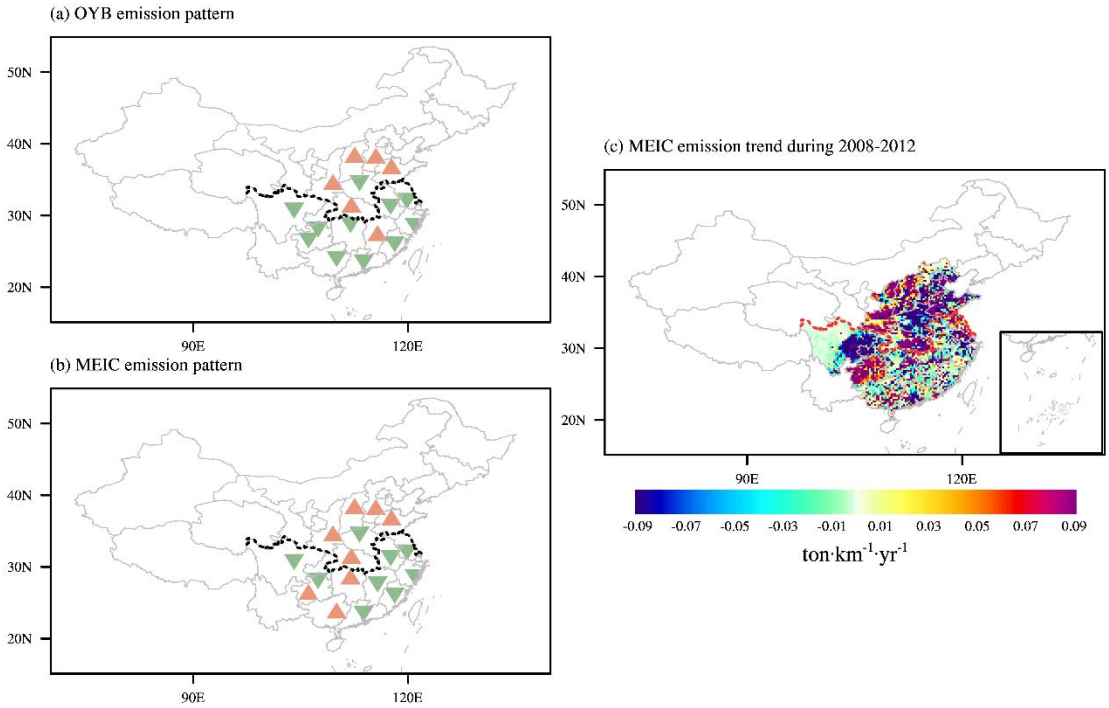

644

645 Figure 9 (left panel) Temporal structure classification of SO_2 emission based on OYB and MEIC. Red

646 upward pointing triangle implies non-monotonic decrease with a rebound in the middle, while monotonic

647 decrease is denoted by green downward pointing triangle. (Right panel) slope of the linear regression of

648 MEIC gridded emission over years 2008, 2010 and 2012. The black or red dotted line delimits the North

649 China and South China.

650

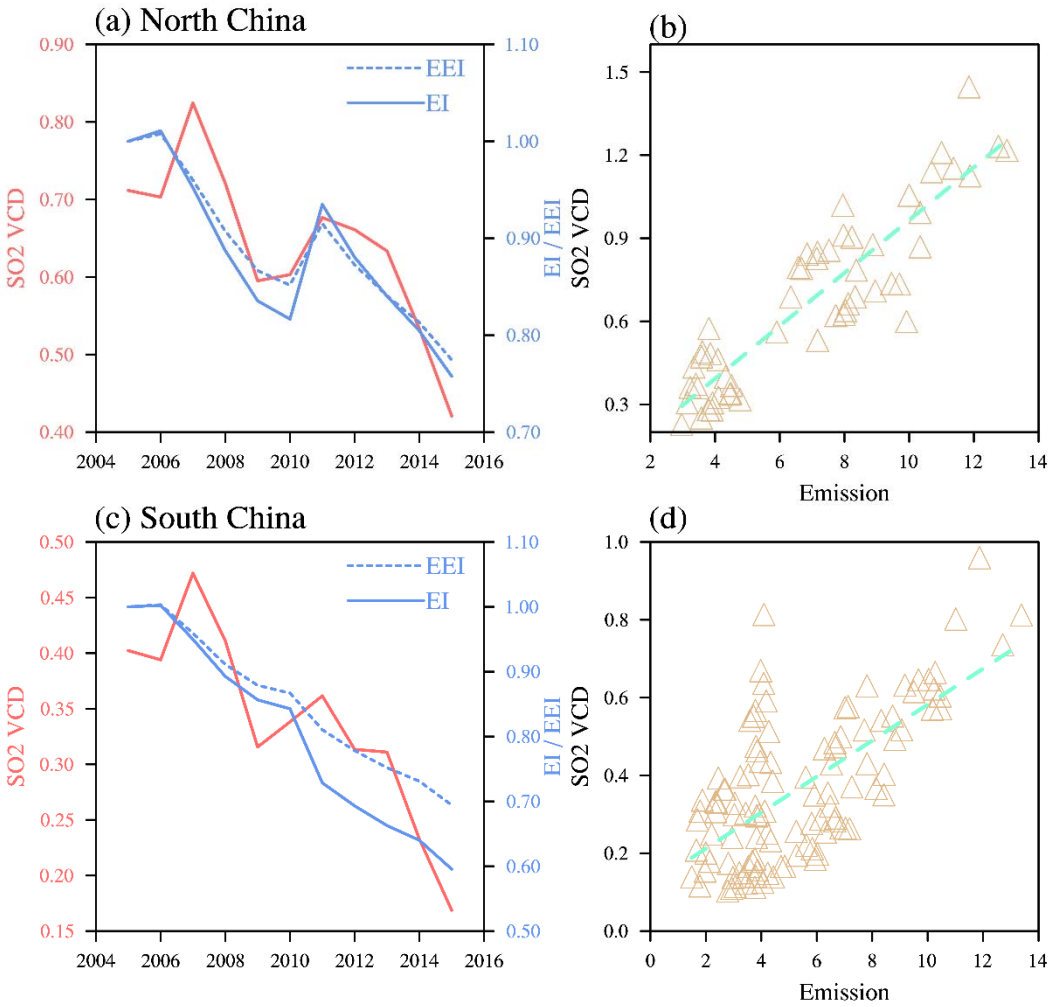

651

652 Figure 10 Time series plots of SO2 VCD and EI/EEI (a, c), and scatter plots with regression line of

653 SO2 VCD and emission (b, d) for North China (1st Row) and South China (2nd Row). Each marker in b

654 and d corresponds to one year and one province.

655

656

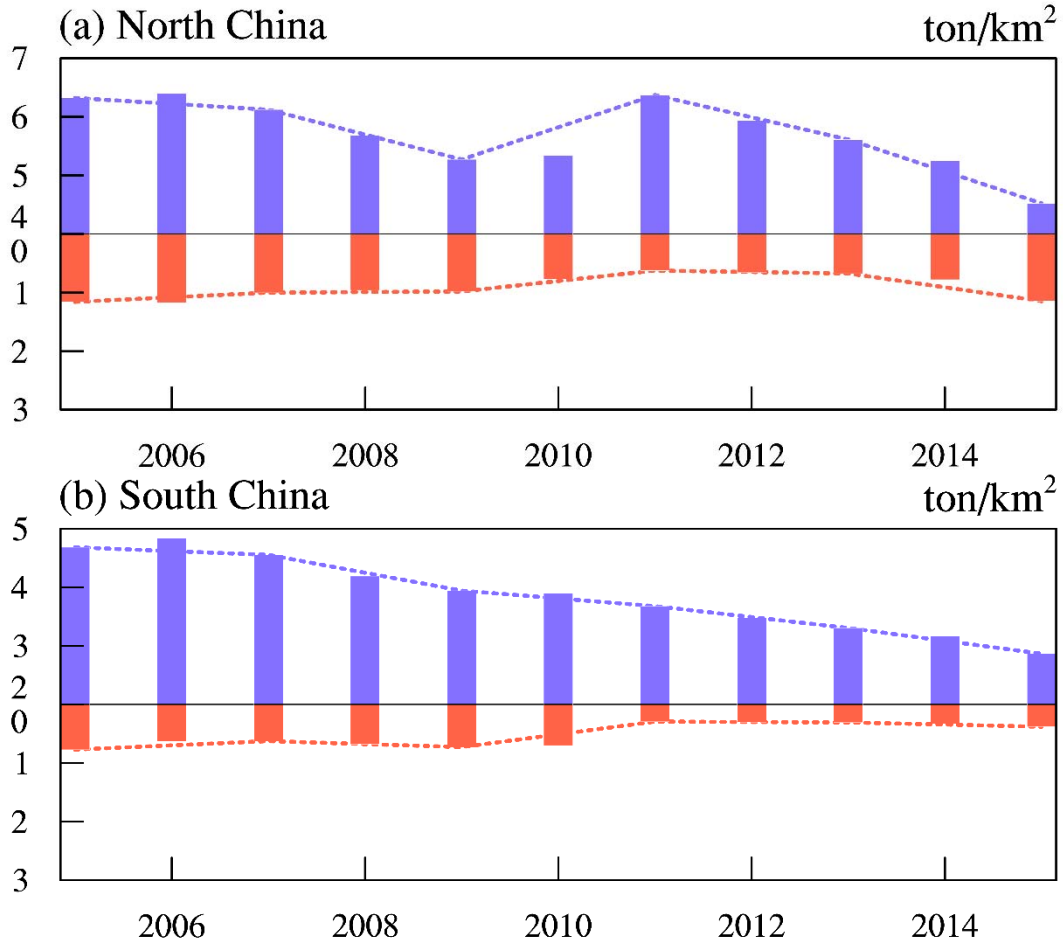

657

658 Figure 11 Annual SO2 emission (ton/km^2) generated by industries (upward blue bars) and households

659 (downward red bars) in North China (a) and South China (b). Notice that the Y-axis in a positive direction

660 does not start at zero.

661

662

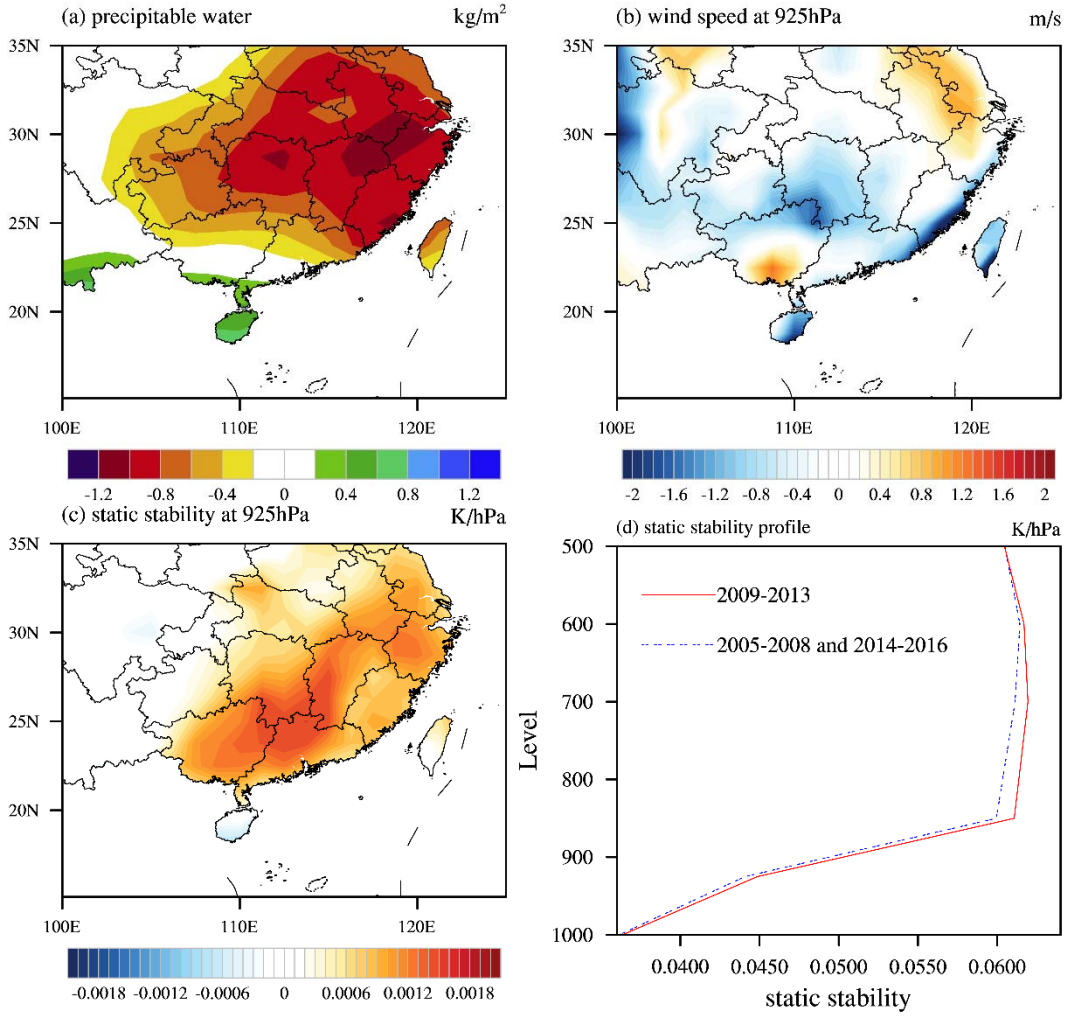

Figure 12 Comparison of atmospheric conditions between the period of 2009-2013 and the other years: (a) composite difference in precipitable water (unit: kg/m^2), (b) composite difference in wind velocity at 925hPa (unit: m/s), (c) composite difference in static stability at 925hPa (unit: K/hPa), and (d) averaged vertical profile of static stability over the 23-31N°, 105-122°N rectangle for the two episodes.